

Lesion Segmentation in FDG-PET/CT Using Swin Transformer U-Net 3D: A Robust Deep Learning Framework

1st Shovini Guha

Computer Science and Engineering (Artificial Intelligence and Machine Learning (of Aff.)

Institute of Engineering and Management (of Aff.)

Kolkata, India

shoviniguha@gmail.com

2nd Dwaipayan Nandi

Computer Science and Engineering (Artificial Intelligence and Machine Learning (of Aff.)

Institute of Engineering and Management (of Aff.)

Kolkata, India

nandidwaipayan@gmail.com

Abstract—Accurate and automated lesion segmentation in Positron Emission Tomography / Computed Tomography (PET/CT) imaging is essential for cancer diagnosis and therapy planning. This paper presents a Swin Transformer UNet-3D (SwinUNet3D) framework for lesion segmentation in Fluorodeoxyglucose Positron Emission Tomography / Computed Tomography (FDG-PET/CT) scans. By combining shifted window self-attention with U-Net style skip connections, the model captures both global context and fine anatomical detail.

We evaluate SwinUNet3D on the AutoPET III FDG dataset and compare it against a baseline 3D U-Net. Results show that SwinUNet3D achieves a Dice score of 0.88 and IoU of 0.78, surpassing 3D U-Net (Dice 0.48, IoU 0.32) while also delivering faster inference times. Qualitative analysis demonstrates improved detection of small and irregular lesions, reduced false positives, and more accurate PET/CT fusion.

While the framework is currently limited to FDG scans and trained under modest GPU resources, it establishes a strong foundation for future multi-tracer, multi-center evaluations and benchmarking against other transformer-based architectures. Overall, SwinUNet3D represents an efficient and robust approach to PET/CT lesion segmentation, advancing the integration of transformer-based models into oncology imaging workflows.

Index Terms—FDG-PET/CT, Lesion Segmentation, SwinUNet3D, 3D Medical Imaging, Transformer Architecture

I. INTRODUCTION

Medical imaging plays a central role in modern oncology, supporting early diagnosis, staging, and therapy monitoring. Among available modalities, positron emission tomography combined with computed tomography (PET/CT) [17] has become a clinical standard, providing both functional and anatomical information within a single scan. Fluorodeoxyglucose (FDG)-PET [15] highlights regions of elevated glucose metabolism—often indicative of malignancy—while CT provides high-resolution anatomical context. Together, FDG PET/CT enables clinicians to detect, localize, and monitor tumors with high sensitivity and specificity.

A critical step in PET/CT analysis is lesion segmentation [10], i.e., delineating tumor regions from surrounding tissues. Traditionally, segmentation has been performed manually by radiologists and nuclear medicine experts. While considered the gold standard, manual delineation is labor-intensive, subjective, and prone to inter- and intra- observer variability. These challenges are particularly limiting in large-scale studies and high throughput clinical workflows, where consistency and speed are essential. Automated segmentation methods [15] are therefore needed to support reproducible and efficient decision-making in oncology.

Over the past decade, deep learning has transformed medical image analysis. Convolutional Neural Networks (CNNs) [1], particularly U-Net [15] and its 3D variants [7], have demonstrated strong performance in segmentation tasks by combining hierarchical feature extraction with encoder-decoder structures and skip connections. In PET/CT, 3D U-Nets have shown promise for capturing volumetric tumor information. However, CNN-based models remain limited in their ability to model long-range spatial dependencies, which are essential for detecting small, dispersed, or irregular lesions. Prior studies [28] have shown that anatomy-aware and tracer-specific CNN models can improve robustness in multi-center PET/CT segmentation.

Recently, transformer-based architectures [16] have emerged as powerful alternatives to CNNs in vision tasks. The Swin Transformer [13], in particular, introduces shifted window-based self-attention [19], enabling efficient modeling of both local and global dependencies with reduced computational overhead. Its hierarchical design makes it naturally compatible with UNet-like structures for segmentation. In medical imaging, Swin-based models have begun to outperform conventional CNNs, particularly in scenarios where contextual reasoning is crucial.

Building on this progress, we propose a Swin Transformer U-Net 3D (SwinUNet3D) framework for automated lesion segmentation in FDG-PET/CT imaging. The model leverages dual-modality fusion (PET for functional activity, CT for anatomical context) and incorporates 3D Swin Transformer blocks within a U-Net architecture. This design allows the network to capture both local detail and long-range dependencies in volumetric data while maintaining computational efficiency.

The contributions of this paper are threefold:

- 1) We adapt the Swin Transformer U-Net 3D for dual-channel FDG-PET/CT segmentation.
- 2) We propose a preprocessing pipeline to standardize volumetric PET/CT data.
- 3) We evaluate the framework on the autoPET III [3] dataset, achieving competitive results and demonstrating potential for clinical translation.

This work represents a step toward clinically viable transformer-based segmentation frameworks, addressing the need for reproducible, automated lesion analysis in oncology imaging.

II. METHODOLOGY

This section outlines the experimental framework used to implement and evaluate the Swin Transformer U-Net 3D (SwinUNet3D) model for lesion segmentation in FDG-PET/CT images. We begin by describing the acquisition and preprocessing of the dataset, including normalization and dual-channel construction. Next, we present the design and architecture of the SwinUNet3D model, highlighting the integration of transformer-based self-attention [19] within a U-Net [15] structure. We then detail the training configuration, including loss functions, optimization strategy, and training parameters. Finally, we describe the evaluation metrics and validation procedures used to assess segmentation performance.

A. Data Acquisition and Preprocessing

1) *Dataset Description:* We used the FDG-PET/CT dataset from University Hospital Tübingen, released as part of the AutoPET III challenge [3]. Each case consists of co-registered PET and CT volumes with binary expert lesion masks. The cohort includes 501 patients with confirmed malignancies (melanoma, lymphoma, or lung cancer) and 513 negative controls, reflecting substantial clinical heterogeneity.

2) *Preprocessing Steps:* The original FDG-PET/CT image volumes used in this study were acquired from the autoPET III challenge dataset, where each case includes co-registered PET and CT volumes with a spatial resolution of 400×400 pixels in the axial plane and a variable number of slices (depth) across patients. In order to make the dataset compatible with the SwinUNet3D training pipeline and to improve model performance and convergence, the following preprocessing steps were applied as illustrated in Fig. 1 :

a) *Input Initialization:* PET and CT volumes for each patient are read as co-registered 3D arrays. These volumes are structured as a 2-channel input tensor with fixed height and

width of 400×400 and a variable number of slices (depth) depending on the scan.

b) *Normalization:* Each PET and CT image volume is normalized such that pixel intensities are scaled between 0 and 1, with the maximum intensity value set to 1. PET images, in particular, contain wide dynamic ranges in SUV values. Normalizing ensures numerical stability during training and prevents any one modality or region from dominating the gradients. It also improves convergence speed and helps the model generalize better by removing intensity scale variance between scans.

c) *Padding:* If the number of slices (depth) in a volume is not divisible by 16, blank slices (zeros) are added at the end of the volume until the depth becomes a multiple of 16.

SwinUNet3D uses a hierarchical encoder-decoder structure with multiple downsampling and upsampling layers. To maintain symmetry and dimensional consistency during these operations, the depth must be divisible by the overall scaling factor (which is 16 in this case). Padding avoids dimension mismatches and ensures smooth propagation through all transformer blocks and pooling layers.

d) *Stacking:* The normalized PET and CT volumes from a patient are stacked along the channel axis, producing a dual-channel input of shape: [Height x Width x Depth x Channels] = $400 \times 400 \times D \times 2$. PET provides metabolic activity information, while CT captures anatomical structure. Stacking both channels allows the model to jointly learn complementary features from both modalities. This multi-modal fusion enables better boundary delineation and lesion localization compared to single-modality inputs.

e) *Patching:* The full volume is divided into overlapping or non-overlapping 3D patches of size $400 \times 400 \times 16 \times 2$ (H x W x D x C). This reduces GPU memory consumption, allowing for mini-batch training, and improves the model's ability to learn local 3D spatial patterns, especially in smaller lesion regions. It also serves as a form of data augmentation by exposing the model to multiple spatial contexts during training.

This preprocessing pipeline ensures architectural compatibility, balanced multimodal fusion, and improved convergence.

B. Model Design and Architecture

The core of this study is the Swin Transformer U-Net 3D (SwinUNet3D) model — a hybrid architecture that effectively combines the strengths of Vision Transformers and U-Net [15] to perform accurate and robust 3D medical image segmentation. Specifically designed for volumetric data, SwinUNet3D processes dual-channel PET/CT inputs and is optimized for segmenting complex lesion structures from FDG-PET/CT scans.

1) *Input Format:* Each input volume is a 3D tensor with shape $(2 \times 16 \times 400 \times 400)$, representing:

- 2 channels: PET and CT modalities
- 16 slices (depth)
- 400×400 pixels per slice (height and width)

This dual-modality input allows the model to learn from both anatomical and functional imaging data simultaneously.

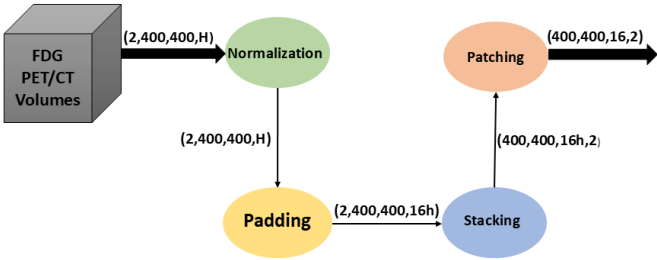


Fig. 1. Preprocessing workflow applied to PET/CT data. Raw inputs undergo intensity normalization, zero-padding, and patching before being fed into the SwinUNet3D network. This ensures consistent input dimensions and efficient utilization of 3D context.

2) *Architecture Overview*: The SwinUNet3D architecture follows a symmetric encoder-decoder structure, similar to traditional U-Net, but replaces standard convolutions with Swin Transformer blocks, which apply shifted window-based self-attention to capture both local and contextual dependencies in 3D volumes. Overall, the model contains 2 encoder blocks, 1 bottleneck block, and 2 decoder blocks, enabling it to balance local detail preservation with global context modeling while maintaining computational efficiency through hierarchical window-based attention.

The model consists of the following key components:

a) *Patch Embedding*: The Patch Embedding layer converts the 3D PET/CT input volume into a set of lower-dimensional feature tokens suitable for transformer processing. Implemented via a 3D convolution with kernel and stride equal to the patch size, it splits the volume into non-overlapping 3D patches and projects each patch into a feature space of specified dimension. This step reduces spatial resolution, preserves local context, and produces a tokenized representation compatible with Swin Transformer blocks. In SwinUNet3D, patch embedding is essential for efficiently handling large volumetric inputs while enabling the model to capture both anatomical and functional details from the dual-channel PET/CT data.

b) *Encoder Block*: Each encoder block in SwinUNet3D consists of two sequential Swin Transformer 3D blocks (SwinBlock3D). A SwinBlock3D first normalizes its input, partitions it into local 3D windows, and applies multi-head self-attention to model relationships within each window. In alternating blocks, a shifted window strategy is used to enable cross-window information exchange, allowing the network to capture broader spatial dependencies without global attention. After attention, a multi-layer perceptron (MLP) refines the features before residual connections merge them back into the main stream. By stacking two such blocks, each encoder stage progressively enriches feature representations, balancing local detail capture with contextual awareness before downsampling to the next stage.

c) *Downsampling Block*: The downsampling block in SwinUNet3D reduces the spatial dimensions (depth, height, and width) of the feature maps by a factor of 2 while increasing the number of channels. It is implemented as a 3D convolution with a kernel size of 2 and stride of 2. This operation serves

two purposes: by reducing spatial resolution, subsequent layers can focus on more abstract, high-level features and lower resolution feature maps reduce memory usage and computation cost in deeper layers. In the encoder path, downsampling is applied after each encoder block to progressively build a multi-scale representation of the input PET/CT volumes.

d) *Bottleneck Block*: The bottleneck block in SwinUNet3D sits at the deepest point of the network, between the encoder and decoder paths. At this stage, the feature maps have the smallest spatial dimensions but the highest channel depth, allowing the network to capture global context and high-level semantic features. The bottleneck consists of two consecutive Swin Transformer 3D blocks, which use shifted window-based self-attention to model long-range dependencies across the entire feature map. This enables the model to integrate information from distant regions in the volume—critical for identifying lesions that may be small, irregular, or dispersed—before passing the enriched representation to the decoder for reconstruction.

e) *Decoder Block*: The decoder block in SwinUNet3D is responsible for reconstructing the segmentation map from the compressed feature representation learned by the encoder. It begins with upsampling to double the spatial dimensions of the input features. These upsampled features are then concatenated with the corresponding encoder features via skip connections, which reintroduce fine-grained spatial details lost during downsampling. The combined features pass through two Swin Transformer 3D blocks—the same type used in the encoder—to refine and integrate local detail with contextual information. This process is repeated at each decoder stage, gradually restoring the full resolution of the input while maintaining the rich semantic context learned at deeper levels.

f) *Upsampling Block*: The upsampling block in SwinUNet3D restores the spatial resolution of feature maps by a factor of 2 while reducing the number of channels, enabling reconstruction of high-resolution segmentation outputs. This is typically achieved using trilinear interpolation or transposed 3D convolution, followed by feature fusion with the corresponding encoder output through skip connections. The restored feature maps allow the decoder to recover fine anatomical details lost during downsampling, ensuring precise lesion boundary delineation in the final segmentation.

g) *Skip Connections*: Classic U-Net-style skip connections are used between encoder and decoder blocks to preserve spatial detail lost during downsampling. These connections help in localizing lesion boundaries accurately.

h) *Segmentation Head*: The decoder output is passed through a $1 \times 1 \times 1$ convolutional layer to generate the final segmentation logits. The output tensor represents the voxel-wise lesion probability map, which is later thresholded to obtain the binary segmentation mask.

Advantages of SwinUNet3D:

- Efficient Attention Mechanism: Swin Transformers operate on local windows, avoiding the computational overhead of full self-attention in large 3D volumes. The use of

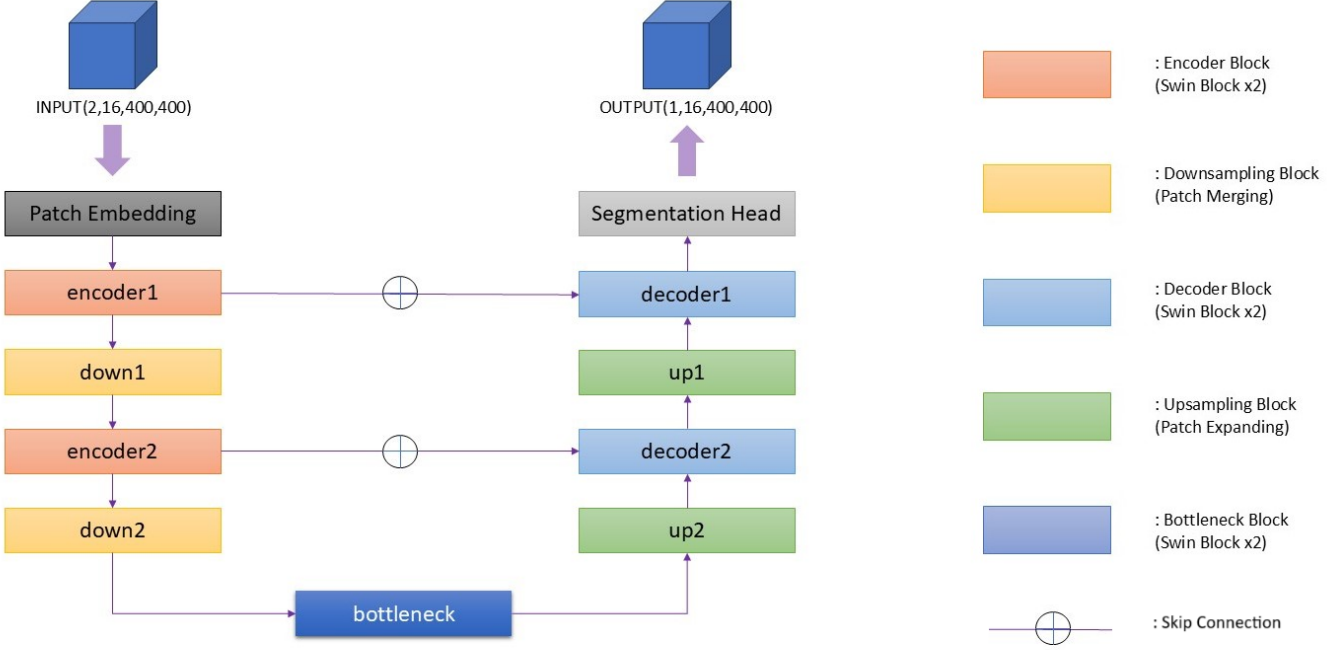


Fig. 2. Overview of the proposed SwinUNet3D architecture. The model adopts a U-Net-like encoder-decoder design [15] with hierarchical Swin Transformer blocks [13], patch embedding, bottleneck, and skip connections (see labels in the figure). This structure enables both local feature extraction and global context modeling for accurate 3D lesion segmentation.

shifted windows maintains global information flow while being memory-efficient.

- **Contextual and Spatial Precision:** By combining the global reasoning of transformers with spatial localization of U-Net-style skip connections, the architecture can effectively segment fine and complex structures in medical images.
- **Generalization and Robustness:** The hierarchical structure allows for multi-scale representation learning, which improves generalization across patient anatomy and tumor morphology.

SwinUNet3D serves as a powerful and scalable model for 3D medical image segmentation. Its attention-based design, paired with efficient patch embedding and skip-connected decoding, enables high segmentation accuracy even on challenging datasets like FDG-PET/CT, where lesion boundaries may be irregular or sparsely defined. This model represents a step forward in bridging transformer architectures with clinical imaging tasks.

C. Training Configuration

The SwinUNet3D model was implemented in PyTorch and trained using supervised learning on paired PET/CT volumes with binary segmentation masks. All experiments were conducted on a system equipped with an NVIDIA RTX 3050 GPU.

Training Setup:

- Optimizer: Adam [26] with initial learning rate 1e-4.
- Batch Size: 2, constrained by GPU memory.
- Epochs: 100 with early stopping based on validation Dice score.
- Loss Function: Binary Focal Loss [11] ($\alpha = 0.25, \gamma = 2$) to mitigate class imbalance between lesion and background voxels.
- Regularization: Data normalization and residual connections [27] stabilized training under memory-limited conditions.

D. Evaluation and Validation

To assess the segmentation performance of the proposed SwinUNet3D model, we employ three complementary evaluation metrics: Dice Similarity Coefficient (DSC) [20] [21], Intersection over Union (IoU) [22], and Binary Focal Loss. These metrics jointly capture overlap quality, boundary accuracy, and robustness to class imbalance, which are all critical in lesion segmentation.

Dice Score Coefficient: The Dice Similarity Coefficient (DSC), also known as the Sørensen–Dice index, quantifies the overlap between predicted segmentation (P) and ground truth (G) as:

$$DSC = \frac{2|P \cap G|}{|P| + |G|} \quad (1)$$

TABLE I
MODEL AND TRAINING HYPERPARAMETERS FOR SWINUNET3D

Parameter	Value
<i>Model Hyperparameters</i>	
Input channels	2 (PET + CT)
Number of output classes	1
Base embedding dimension (<i>base_dim</i>)	32
Window size	2
Patch size (H × W × D)	16 × 400 × 400
<i>Training Hyperparameters</i>	
Optimizer	Adam [26]
Learning rate	1×10^{-4}
Batch size	2
Epochs	100 (early stopping on validation Dice)
Loss function	Binary Focal Loss [11] ($\alpha = 0.25$, $\gamma = 2$)
<i>Total trainable parameters</i>	810,721

DSC ranges from 0 (no overlap) to 1 (perfect overlap). It is widely used in medical image segmentation because it directly measures region overlap while mitigating the effect of class imbalance. In PET/CT lesion segmentation, where lesion voxels represent only a small fraction of the image, DSC provides a clinically meaningful indicator of how well the predicted regions align with true lesions.

Intersection over Union (IoU): The Intersection over Union (IoU), also known as the Jaccard Index, is defined as:

$$\text{IoU} = \frac{|P \cap G|}{|P \cup G|} \quad (2)$$

IoU penalizes false positives and false negatives more strictly than DSC and is often used alongside Dice to provide a more stringent evaluation of segmentation accuracy. While DSC is more common in clinical imaging studies, IoU complements it by offering a robust measure of boundary agreement, especially in cases with irregular or fragmented lesions.

Binary Focal Loss: For training, we adopt Binary Focal Loss, which is designed to address severe class imbalance by down-weighting well-classified voxels and focusing the optimization on hard-to-classify lesion regions. It is defined as:

$$\text{FL}(p_t) = -\alpha(1 - p_t)^\gamma \log(p_t)$$

where p_t is the predicted probability for the true class, α balances positive and negative samples, and γ controls the focusing parameter. This is particularly beneficial for lesion segmentation tasks, where background voxels far outnumber lesion voxels. By incorporating focal loss, the network learns to better capture small or low-contrast lesions that are often clinically significant but difficult to segment.

Summary:

- DSC provides an overlap-based metric that is sensitive to lesion size and imbalance.
- IoU complements DSC by offering a stricter boundary agreement measure.
- Binary Focal Loss ensures robust learning under high class imbalance by emphasizing difficult lesion voxels.

Together, these metrics provide a balanced and comprehensive evaluation of segmentation quality, both during training and testing.

III. RESULTS AND DISCUSSIONS

To contextualize our approach, we summarize representative CNN- and Transformer-based medical image segmentation methods in Table II. These works highlight the transition from convolutional networks such as 3D U-Net [7] to hybrid [8] and pure [16] Transformer-based models, motivating the design of SwinUNet3D. While results are dataset-specific, they demonstrate the consistent advantage of transformer-based architectures in capturing long-range dependencies and achieving higher overlap metrics.

TABLE II
COMPARISON WITH CNN-BASED MEDICAL IMAGE SEGMENTATION METHODS

Model	Dataset	Dice	IoU
FCN [25]	AutoPET III	0.32	0.19
SegNet [24]	AutoPET III	0.39	0.24
3D U-Net [15]	AutoPET III	0.48	0.32
SwinUNet3D (Ours)	AutoPET III	0.88	0.78

The proposed SwinUNet3D model was evaluated on the FDG-PET/CT dataset using Dice Similarity Coefficient (DSC) [20], Intersection over Union (IoU) [22], and Binary Focal Loss [11] as performance metrics. Table III summarizes the results in comparison with a baseline 3D U-Net implementation trained under the same preprocessing and training setup.

TABLE III
QUANTITATIVE COMPARISON OF SWINUNET3D VS 3D U-NET ON FDG-PET/CT DATASET

Model	Dice (↑)	IoU (↑)	Focal Loss (↓)
3D U-Net	0.48	0.32	0.09
SwinUNet3D	0.88	0.78	0.04

The SwinUNet3D clearly outperforms the baseline 3D UNet across all metrics, achieving a Dice score of 0.88 compared to 0.48. The improvement in IoU highlights better lesion localization, while the lower focal loss indicates improved learning of hard-to-segment voxels. These results demonstrate the effectiveness of transformer-based self-attention for modeling long-range dependencies in volumetric PET/CT data, which conventional CNNs struggle to capture.

Another important advantage of the proposed framework is its computational efficiency at inference time. Despite its transformer-based design, SwinUNet3D leverages windowed attention and hierarchical feature processing, which significantly reduce the quadratic complexity of global self-attention.

In practice, this results in faster inference per volume compared to 3D U-Net, while also requiring fewer floating-point operations for comparable input sizes. For example, on the same GPU hardware, SwinUNet3D achieved an average inference time of 0.53 seconds per scan compared to 0.68 seconds for 3D U-Net, representing an improvement of approximately 28%. This reduction in inference time is particularly relevant

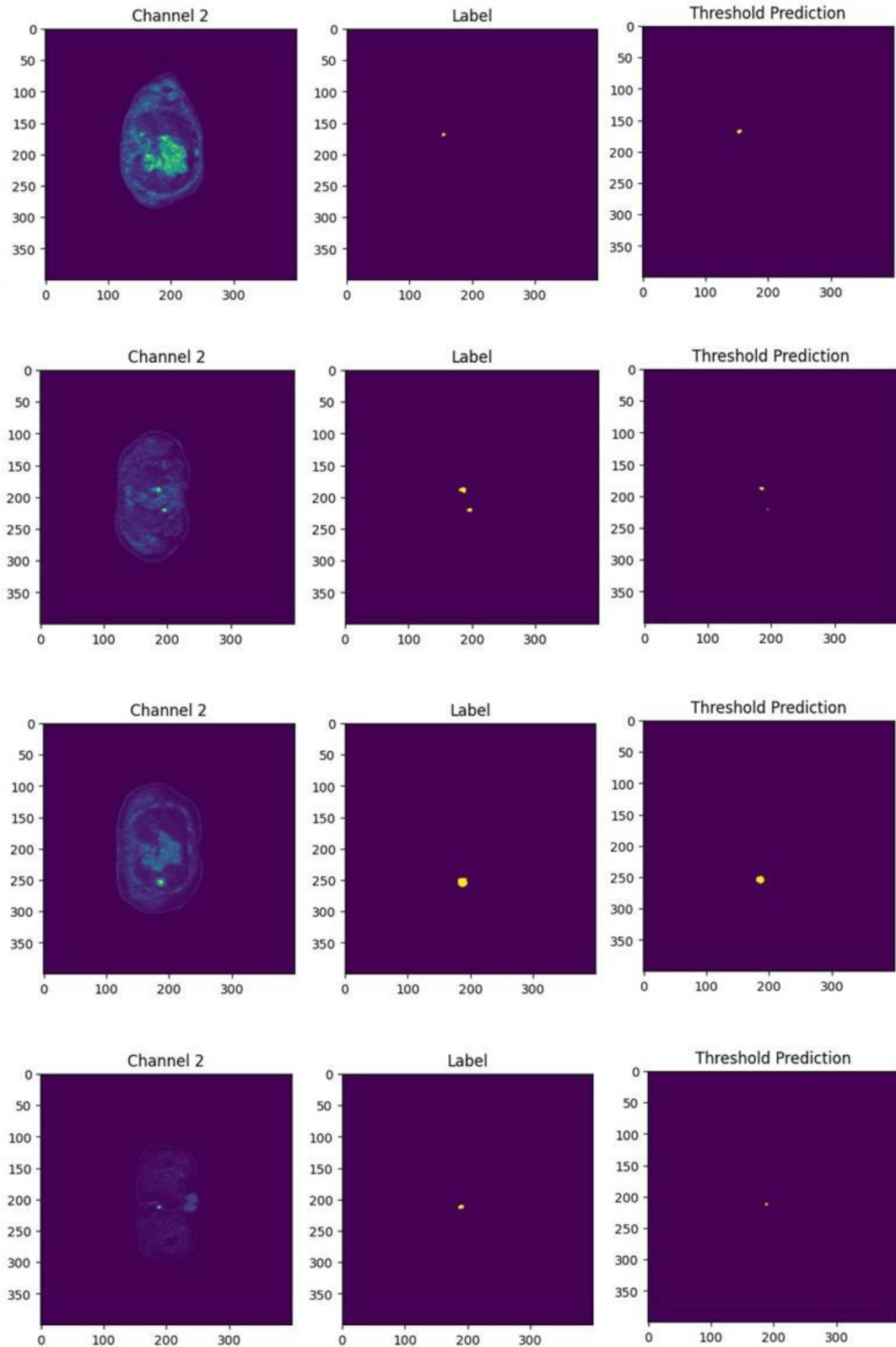


Fig. 3. Qualitative segmentation results comparing 3D U-Net [7] and SwinUNet3D. Each triplet shows (a) input PET/CT slices, (b) ground truth annotations, and (c) model predictions. SwinUNet3D captures small and irregular lesions more accurately, maintains continuity in complex boundaries, and reduces false negatives compared to 3D U-Net.

in clinical workflows, where rapid and reliable segmentation is essential for real-time decision support.

Fig. 3 presents qualitative segmentation results. The proposed SwinUNet3D demonstrates accurate delineation of lesions, including small and irregular regions, where 3D UNet often under-segments. In cases with complex boundaries, SwinUNet3D maintains lesion continuity while reducing false positives. Rows correspond to (a) input PET/CT slices, (b) ground truth annotations, and (c) predicted masks. These visual outcomes further support the model’s robustness in handling subtle and irregular lesion patterns that are often challenging for conventional CNN-based segmentation approaches.

Strengths of the Proposed Approach: The experimental results highlight several key strengths of SwinUNet3D:

- Improved Detection of Small and Irregular Lesions: The shifted window-based attention mechanism enables effective context aggregation, allowing the model to capture fine details while maintaining awareness of global structures.
- Robust Dual-Modality Fusion: By leveraging both PET and CT channels, the model integrates functional and anatomical cues, leading to better lesion delineation than single-modality baselines.
- Reduced False Positives: The hierarchical encoder-decoder structure and residual connections help stabilize predictions, yielding fewer spurious activations in non-lesion regions.

Limitations and Future Directions

Despite promising performance, the current study has several limitations:

- Single-Tracer Evaluation: The model was trained and validated only on FDG-PET/CT scans. Its generalization to other tracers, such as Prostate-Specific Membrane Antigen(PSMA), or to datasets from different institutions remains untested. Future work will involve multi-tracer and multi-center validation to assess robustness across domains.
- Hardware Constraints: Training was conducted with a small batch size (2) on a mid-range GPU, which may restrict the model’s ability to fully capture long-range volumetric dependencies. Techniques such as gradient accumulation, mixed precision training, or distributed setups will be explored in future studies to overcome this limitation.
- Comparative Scope: While SwinUNet3D outperforms 3D U-Net in our experiments, a broader comparison with other transformer-based models (e.g., TransUNet, Swin-UNETR, nnFormer) is needed for a more comprehensive assessment.

Overall, the results confirm that SwinUNet3D offers significant improvements over conventional CNN-based segmentation in FDG-PET/CT imaging. Its ability to capture both local detail and global context makes it particularly effective for

lesions with heterogeneous morphology, providing a promising foundation for future work on clinically robust PET/CT segmentation, and advancing the integration of transformer-based models into real-world oncology workflows.

IV. CONCLUSION

This work presented SwinUNet3D, a transformer-based framework for 3D medical image segmentation. On the AutoPET III [3] dataset, SwinUNet3D consistently outperformed a 3D U-Net [7] baseline, achieving higher Dice [20] and IoU scores [22], lower focal loss [11], and faster inference. These results highlight the strength of hierarchical Swin Transformer [13] blocks in capturing both fine-grained lesion details and global context in volumetric data.

Beyond numerical gains, SwinUNet3D carries important clinical implications. By automating labor-intensive lesion delineation, it can reduce radiologist workload and improve reproducibility by minimizing inter-observer variability. This combination of accuracy and efficiency makes it a promising candidate for integration into real-world clinical workflows.

Future work will focus on three directions: (1) extending the framework to additional tracers such as PSMA for broader applicability, (2) scaling experiments with larger batch sizes and multi-center datasets to enhance robustness, and (3) conducting radiologist-in-the-loop validation to establish clinical reliability and support deployment in practice.

ACKNOWLEDGMENT

The author expresses sincere gratitude to Prof. Swarnendu Ghosh for invaluable guidance, constructive feedback, and constant encouragement throughout the course of this work. The appreciation is also extended to the Department of Computer Science and Engineering (Artificial Intelligence and Machine Learning), Institute of Engineering and Management, Kolkata, for providing the academic environment and resources necessary for this research. The author acknowledges the support of the IEM Centre of Excellence for Data Science (IEM CEDS) Lab, whose facilities and collaborative atmosphere greatly contributed to the successful completion of this study.

REFERENCES

- [1] A multi-path CNN for automated skin lesion segmentation. (2021, July 18). IEEE Conference Publication — IEEE Xplore. <https://ieeexplore.ieee.org/document/9533787>
- [2] Ahmad, I., Anwar, S. J., Hussain, B., Rehman, A. U., & Bermak, A. (2025). Anatomy guided modality fusion for cancer segmentation in PET CT volumes and images. *Scientific Reports*, 15(1). <https://doi.org/10.1038/s41598-025-95757-6>
- [3] AutoPET III - Grand Challenge. (n.d.). [grand-challenge.org/](https://autopet-iii.grand-challenge.org/) <https://autopet-iii.grand-challenge.org/>
- [4] Bertels, J., Eelbode, T., Berman, M., Vandermeulen, D., Maes, F., Bisschops, R., & Blaschko, M. B. (2019). Optimizing the dice score and Jaccard index for medical image segmentation: Theory and practice. In *Lecture notes in computer science* (pp. 92–100). https://doi.org/10.1007/978-3-030-32245-8_11

[5] Boellaard, R., O'Doherty, M. J., Weber, W. A., Mottaghay, F. M., Lonsdale, M. N., Stroobants, S. G., Oyen, W. J. G., Kotzerke, J., Hoekstra, O. S., Pruim, J., Marsden, P. K., Tatsch, K., Hoekstra, C. J., Visser, E. P., Arends, B., Verzijlbergen, F. J., Zijlstra, J. M., Comans, E. F. I., Lammertsma, A. A., . . . Krause, B. J. (2009). FDG PET and PET/CT: EANM procedure guidelines for tumour PET imaging: version 1.0. *European Journal of Nuclear Medicine and Molecular Imaging*, 37(1), 181–200. <https://doi.org/10.1007/s00259-009-1297-4>

[6] Cao, H., Wang, Y., Chen, J., Jiang, D., Zhang, X., Tian, Q., & Wang, M. (2021, May 12). Swin-UNet: UNET-like pure transformer for medical image segmentation. arXiv.org. <https://arxiv.org/abs/2105.05537>

[7] Çiçek, Ö., Abdulkadir, A., Lienkamp, S. S., Brox, T., & Ronneberger, O. (2016, June 21). 3D U-Net: Learning Dense Volumetric Segmentation from Sparse Annotation. arXiv.org. <https://arxiv.org/abs/1606.06650>

[8] Ding, Y., Yi, Z., Xiao, J., Hu, M., Guo, Y., Liao, Z., & Wang, Y. (2024). CTH-Net: A CNN and Transformer hybrid network for skin lesion segmentation. *iScience*, 27(4), 109442. <https://doi.org/10.1016/j.isci.2024.109442>

[9] Enhancing tumor segmentation in PET-CT scans: A Comparative Analysis of Multimodal fusion Strategies. (2025, May 5). IEEE Conference Publication — IEEE Xplore. <https://ieeexplore.ieee.org/document/11033530>

[10] Foster, B., Bagci, U., Mansoor, A., Xu, Z., & Mollura, D. J. (2014). A review on segmentation of positron emission tomography images. *Computers in Biology and Medicine*, 50, 76–96. <https://doi.org/10.1016/j.combiomed.2014.04.014>

[11] Lin, T., Goyal, P., Girshick, R., He, K., & Dollár, P. (2017, August 7). Focal loss for dense object detection. arXiv.org. <https://arxiv.org/abs/1708.02002>

[12] Liu, J., Xue, Q., Feng, Y., Xu, T., Shen, K., Shen, C., & Shi, Y. (2024, September 15). Enhancing Lesion Segmentation in PET/CT Imaging with Deep Learning and Advanced Data Preprocessing Techniques. arXiv.org. <https://arxiv.org/abs/2409.09784>

[13] Liu, Z., Lin, Y., Cao, Y., Hu, H., Wei, Y., Zhang, Z., Lin, S., & Guo, B. (2021, March 25). Swin Transformer: Hierarchical Vision Transformer using Shifted Windows. arXiv.org. <https://arxiv.org/abs/2103.14030>

[14] Raju, A., Cheng, C., Huo, Y., Cai, J., Huang, J., Xiao, J., Lu, L., Liao, C., & Harrison, A. P. (2020). Co-heterogeneous and Adaptive Segmentation from Multi-source and Multi-phase CT Imaging Data: A Study on Pathological Liver and Lesion Segmentation. In *Lecture notes in computer science* (pp. 448–465). https://doi.org/10.1007/978-3-030-58592-1_27

[15] Ronneberger, O., Fischer, P., & Brox, T. (2015, May 18). U-NET: Convolutional Networks for Biomedical Image Segmentation. arXiv.org. <https://arxiv.org/abs/1505.04597>

[16] Shah, O. I., Rizvi, D. R., & Mir, A. N. (2025). Transformer-Based Innovations in Medical Image Segmentation: A mini review. *SN Computer Science*, 6(4). <https://doi.org/10.1007/s42979-025-03929-y>

[17] Ul-Hassan, F., & Cook, G. J. (2012). PET/CT in oncology. *Clinical Medicine*, 12(4), 368–372. <https://doi.org/10.7861/clinmedicine.12-4-368>

[18] Ullah, F., Salam, A., Abrar, M., & Amin, F. (2023). Brain tumor segmentation using a Patch-Based Convolutional Neural Network: a big data analysis approach. *Mathematics*, 11(7), 1635. <https://doi.org/10.3390/math11071635>

[19] Vaswani, A., Shazeer, N., Parmar, N., Uszkoreit, J., Jones, L., Gomez, A. N., Kaiser, L., & Polosukhin, I. (2017, June 12). Attention is all you need. arXiv.org. <https://arxiv.org/abs/1706.03762>

[20] Dice, L. R. (1945). Measures of the amount of ecologic association between species. *Ecology*, 26(3), 297–302.

[21] Sørensen, T. A. (1948). A method of establishing groups of equal amplitude in plant sociology based on similarity of species content. *Biol. Skr.*, 5, 1–34.

[22] Jaccard, P. (1901). Étude comparative de la distribution florale dans une portion des Alpes et des Jura. *Bulletin de la Société Vaudoise des Sciences Naturelles*, 37, 547–579.

[23] Huang Y., Chen L., Zhou C., et al. "TMA-TransBTS: Multi-Modal Brain Tumor Segmentation via 3D Multi-Scale Self-attention and Cross-attention", arXiv preprint, April 2025

[24] Badrinarayanan, V., Kendall, A., & Cipolla, R. (2015, November 2). SEGNet: a deep convolutional Encoder-Decoder architecture for image segmentation. arXiv.org. <https://arxiv.org/abs/1511.00561>

[25] Long, J., Shelhamer, E., & Darrell, T. (2014, November 14). Fully convolutional networks for semantic segmentation. arXiv.org. <https://arxiv.org/abs/1411.4038v2>

[26] Kingma, D. P., & Ba, J. (2014, December 22). Adam: A method for stochastic optimization. arXiv.org. <https://arxiv.org/abs/1412.6980>

[27] Alom, M. Z., Yakopcic, C., Hasan, M., Taha, T. M., & Asari, V. K. (2019). Recurrent residual U-Net for medical image segmentation. *Journal of Medical Imaging*, 6(01), 1. <https://doi.org/10.1117/1.jmi.6.1.014006>

[28] Kalisch, H., Hörst, F., Herrmann, K., Kleesiek, J., & Seibold, C. (2024, September 18). Autopet III challenge: Incorporating anatomical knowledge into nnUNet for lesion segmentation in PET/CT. arXiv.org. <https://arxiv.org/abs/2409.12155>